Int. J. Electrochem. Sci., 14 **(2019)** 6920 – 6937, doi: 10.20964/2019.07.74

International Journal of
ELECTROCHEMICAL
SCIENCE
www.electrochemsci.org

Synergistic Effect on the Electrochemical Performances of Polypyrrole Nanoparticles Distributed on the Graphene Layers as an Electrodes for Supercapacitors

Sarah Umeera Muhamad[1], *Nurul Hayati Idris*[1,*] *and M. F. Md Din*[2]

[1] Energy Storage Research Group, School of Ocean Engineering, Universiti Malaysia Terengganu, 21030 Kuala Nerus, Terengganu, Malaysia
[2] Department of Electrical & Electronic Engineering, Faculty of Engineering, National Defence University of Malaysia, Kem Sungai Besi, 57000 Kuala Lumpur, Malaysia.
[*]E-mail: nurulhayati@umt.edu.my

Received: 15 October 2018 / *Accepted:* 9 May 2019 / *Published:* 10 June 2019

The polypyrrole (PPy) nanoparticles distributed on the graphene layers are prepared via *in-situ* polymerization method. The amount of PPy on the graphene layers is varied in order to obtain the highest electrochemical performances. The PPy in graphene/PPy refers to nanoparticles with a diameter size of 0.19 µm. The graphene/PPy exhibited excellent electrochemical performances when 80 wt.% of PPy was added into the composite, with specific capacitance of approximately 270 F g^{-1} at a current density of 500 mA g^{-1}. Furthermore, 77% of initial capacitance was retained after 1000 charge/discharge cycles, which suggests good cycling stability of the composite at a current density of 5000 mA g^{-1}. The improved electrochemical performances of the composite are attributable to the synergistic effect of the PPy nanoparticles and crumpled graphene layers, which gave large surface area, short ion diffusion pathway, excellent rate performance, and cycling stability.

Keywords: supercapacitor; graphene; polypyrrole; synergistic effect; capacitance

1. INTRODUCTION

Energy storage has attracted intensive research efforts in recent years with the global demand for renewable energy production due to the rapid consumption of fossil fuel and serious environmental pollution. Supercapacitor is one of the attractive energy storage devices due to its important features, such as high power density, fast charging/discharging processes (within seconds), and long cycle life [1-3]. Supercapacitor is classified according to two charge storage mechanisms; electrical double layer capacitor (EDLC) and pseudocapacitance of Faradaic reactions. High specific surface area materials, such as porous carbon [4-9], carbon aerogels [10-12], and graphene [13-15], have shown promising

EDLC performances by providing excellent conductivity and good cyclability. Meanwhile, transition metal oxides [16-18] and conducting polymers [19, 20] are fundamental candidates used as electrode materials for pseudocapacitor. Conducting polymers are more capable to be used as an electrode for pseudocapacitor since these materials are low in cost, environmental-friendly, and easy-to-synthesis. However, they are limited in applications due to poor mechanical properties and performance stability during charge/discharge process [21]. Therefore, hybridising conducting polymers to carbon-based materials has become an effective strategy to improve the cycling stability of the conducting polymers [22-24]. Moreover, the conducting polymers possess higher specific capacitance than that of carbon-based materials [1, 3, 25]. Graphene was chosen as the carbon-based materials owing to the ease of synthesis, cost effective, remarkable mechanical stiffness, large surface area and excellent electrical conductivity [26-28] and has been explored by several researchers.

Table 1. Comparison of the supercapacitor performances based on graphene/PPy composite materials.

Composites	Synthesis method	Electrolyte	Specific capacitance ($F\ g^{-1}$)	Reference
Graphene/PPy	In situ polymerization	1 M H_2SO_4	650 at 0.45 A g^{-1}	[32]
RGO/PPy	Electropolymerization	1 M H_2SO_4	424 at 1 A g^{-1}	[51]
Graphene/PPy nanowire	Chemical polymerization	1 M NaCl	165 at 1 A g^{-1}	[19]
Graphene nanosheets/PPy	In-situ polymerization	1 M H_2SO_4	482 at 0.5 A g^{-1}	[42]
Graphene sheets/PPy	Chemical polymerization	2 M H_2SO_4	400 at 0.3 A g^{-1}	[52]
RGO/PPy	In-situ polymerization	-	249 at 0.3 A g^{-1}	[25]
RGO/PPy	In-situ oxidation polymerization	1M H_2SO_4	420 at 0.1 A g^{-1}	[53]
Exfoliated graphene /PPy	One-step electrochemical exfoliation	3M KCl	351 at 1 A g^{-1}	[54]

Table 1 lists the specific capacitance of graphene/PPy in various electrolyte. Conducting polymers also can be easily prepared through polymerisation method and the electrical properties of the conducting polymers can be modulated with the presence of acid and the subsequent doping of the anion counterpart of acid during the polymerisation process [25]. Hence, the PPy obtained in these studies seemed to appear in bulk with micrometre sizes. The capacitance of graphene/PPy composites strongly

depends on the synthesis methods of graphene and PPy, as well as the morphology and particle size of the composites.

Inspired by prior studies, a facile strategy is proposed to prepare graphene/PPy composites via *in-situ* polymerisation method using water as solvent. Graphene can be easily incorporated with conducting polymers as a precursor to improve the electrochemical properties of the composites due to its synergistic effect and to provide considerable advantages, such as increased electrical conductivity, robust mechanical/chemical stability, and reduced agglomeration. Herein, graphene does not only serve as a highly conductive support material, but it also offers a large surface area for well-dispersed deposition of the PPy nanoparticles. Furthermore, the linkage between PPy nanoparticles and graphene layers could shorten the ions diffusion pathway. In addition, PPy nanoparticles deposited on graphene layers can minimise the restacking of graphene layers. This research demonstrates the optimum composition of PPy nanoparticles decorated on the graphene layers in order to maximise the electrochemical performances of the hybrid materials as a promising electrode for supercapacitor.

2. EXPERIMENTAL SECTION

2.1. Preparation of graphite oxide and graphene

Graphite oxide (GO) was prepared by using the Hummer's method as reported in the literature [29]. First, 1 g graphite (Aldrich) was added into 50 mL H_2SO_4 (Sigma-Aldrich, 95-97%) in ice-bath and the mixture was stirred for 10 min. Then, 6 g $KMnO_4$ (Sigma-Aldrich, ≥ 99%) was slowly added under vigorously stirring and heated at 30 °C for 1 h. Next, 80 mL deionised water was added and the temperature was increased up to 90 °C for 30 min. The reaction was terminated by adding 200 mL deionised water, followed by 6 mL H_2O_2 (Merck Schuchardt OHG, 30%). The mixture was centrifuged and the precipitate was washed several times with HCl (Merck, 37 %) and acetone (Emsure). Finally, the GO was dried at 65 °C for 12 h under vacuum.

Next, the GO was reduced to graphene. Specifically, 0.6 g GO powder was added into 200 mL ethanol (HmbG chemicals, 99.6 %) and underwent ultrasonic for 1 h to obtain a yellow-brownish solution. Then, 10 mL N_2H_4 (Sigma-Aldrich, 50-60 %) was added dropwise at 60 °C under vigorous stirring for 15 min. The mixture was centrifuged and washed several times with deionised water and ethanol, in which the black precipitate was dried at 60 °C for 12 h under vacuum.

2.2. Preparation of graphene/PPy

The graphene/PPy composites were prepared by using the *in-situ* polymerisation method. The first solution containing 0.2417 g $FeCl_3$ (Sigma-Aldrich, 97 %) was dissolved in 96.5 mL deionised water. The second solution was prepared by dispersing 0.6 g graphene in 100 mL deionised water and underwent ultrasonic for 1 h. Next, pyrrole (Aldrich, 98 %) was added into graphene suspension. The first solution was added dropwise into the second solution under ice-bath and stirred for 24 h. Then, the black precipitate was washed several times with deionised water and ethanol. The different weight ratios

of PPy in the graphene/PPy composites were prepared. For 20, 40, and 80 wt.% PPy in the graphene/PPy composites; 0.0001 M, 0.0002 M, and 0.0004 M pyrrole had been added into the second solution, respectively.

2.3. Material characterisation

The X-ray diffraction (XRD) of graphene/PPy was measured using (Rigaku Miniflex II) with monochromatic Cu-Kα radiation (λ = 1.5406 Å). The Fourier transform infrared (FTIR) spectrum was obtained on an IR Tracer-100 spectrophotometer (SHIMADZU). The scanning electron microscope (SEM) (JEOL JSM-6360LA) and transmission electron microscope (TEM) (JEOL 2100-F) were used to investigate the morphology of the graphene/PPy composites. Raman spectra were perfromed on Renishaw Raman spectroscopy (532 nm radiation) extended with 0.1% power laser measurement.

2.4. Electrochemical measurements

The electrochemical measurements were carried out in a three-electrode system using Autolab PGSTAT302 (Eco-Chemie) in a voltage range from –0.2 to 0.8 V. A platinum rod was used as a counter electrode, a saturated calomel electrode was used as a reference electrode and 1 M sulphuric acid (H_2SO_4) (Sigma-Aldrich, 95–98%) aqueous solution was used as the electrolyte. Then, the working electrode was prepared by dissolving of 75 wt% graphene/PPy composites, 20 wt% carbon black (Sigma-Aldrich), and 5 wt% polyvinylidene fluoride (PVDF) (Sigma-Aldrich) in *N*-methyl-2-pyrrolidone (NMP) (Sigma-Aldrich). The slurry was pasted onto a titanium foil and dried at 100 °C under vacuum.

3. RESULTS AND DISCUSSION

The XRD patterns of graphene layers, PPy nanoparticles, and graphene/PPy composites are illustrated in Fig. 1.

The broad peak exhibited at 2θ of 26º indicates the amorphous nature of PPy [30]. The diffraction peaks at 2θ of 24.5º and 43º assigned to graphene layers appeared in the graphene/PPy composites. Due to the amorphous state of PPy, these peaks turned broader with the increased amount of PPy. In order to confirm the existence of PPy in the graphene/PPy composites, FTIR and Raman spectroscopy were performed.

The FTIR spectra of the graphene layers, PPy nanoparticles, and graphene/PPy composites are displayed in Fig. 2. The IR peaks of graphene layers agreed well with those in the literature [31], where the peak at 1552 cm^{-1} can be assigned to the C=C stretching vibration and the peak at 1192 cm^{-1} is attributed to the C-C bond.

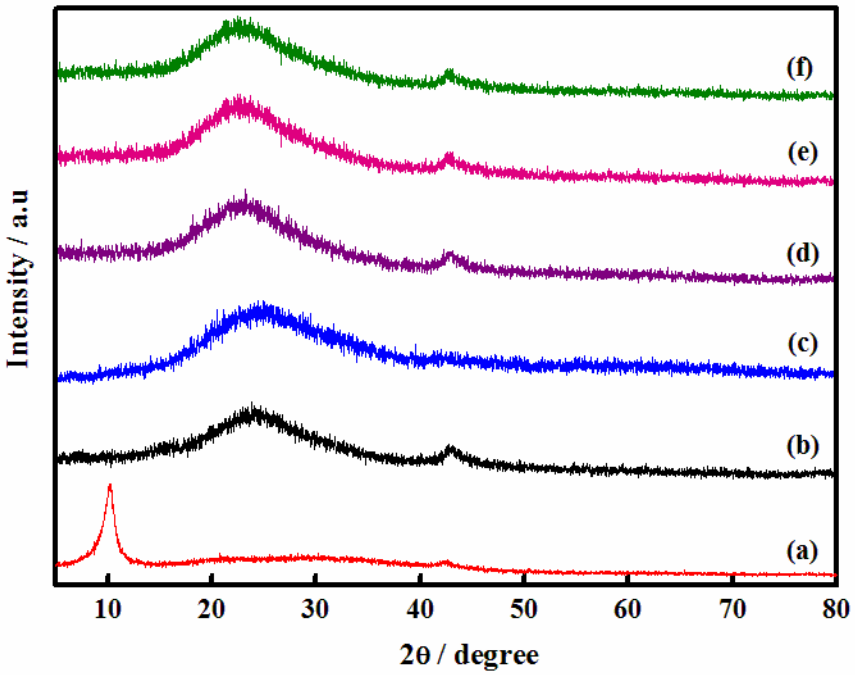

Figure 1. XRD patterns of (a) GO, (b) graphene layers, (c) PPy nanoparticles, (c) graphene/PPy 20 wt.%, (d) graphene/PPy 40 wt.%, (f) graphene/PPy 80 wt.%.

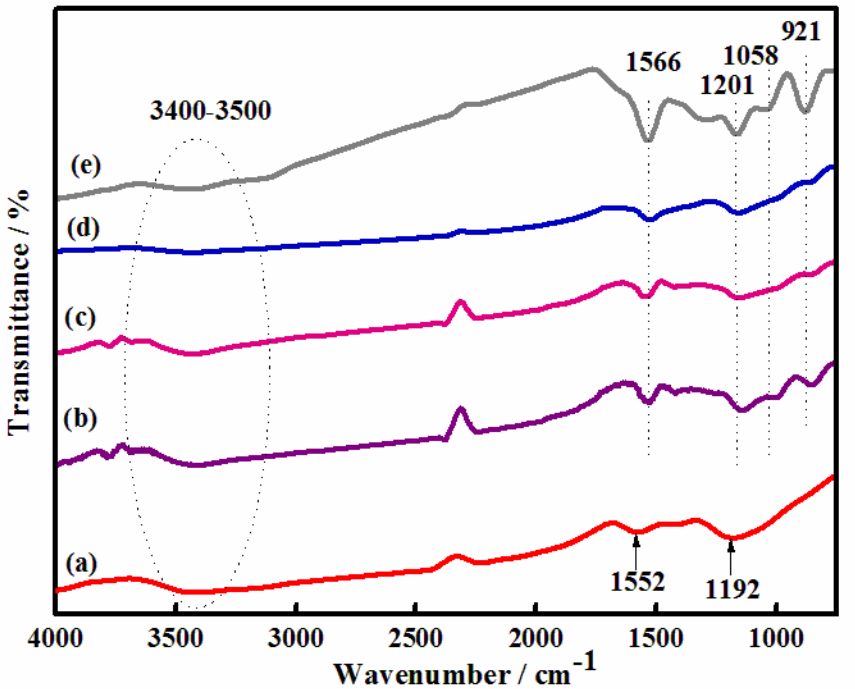

Figure 2. FTIR spectra of (a) graphene layers, (b) graphene/PPy 80 wt.%, (c) graphene/PPy 40 wt.%, (d) graphene/PPy 20 wt.% and (e) PPy nanoparticles.

Meanwhile, the broad peaks around 3400-3500 cm^{-1} can be assigned to the O-H stretching vibration. These peaks were also observed in graphene/PPy composites, however became more intense;

indicating the interaction between PPy nanoparticles and graphene layers, such as hydrogen bonding and π-π stacking between them [32]. As for the PPy nanoparticles, the characteristic band at 1566 cm^{-1} can be ascribed to the stretching vibration of pyrrole rings. In addition, the peaks located at 1201 cm^{-1} and 921 cm^{-1} are ascribed to the C-N stretching and the doping state of PPy, respectively, while the band at 1058 cm^{-1} can be attributed to C-H [33]. The C-H and N-H stretching vibrations are difficult to distinguish in the graphene/PPy composites because these peaks overlap with the O-H stretching vibration of graphene in the region of 3400-3500 cm^{-1}.

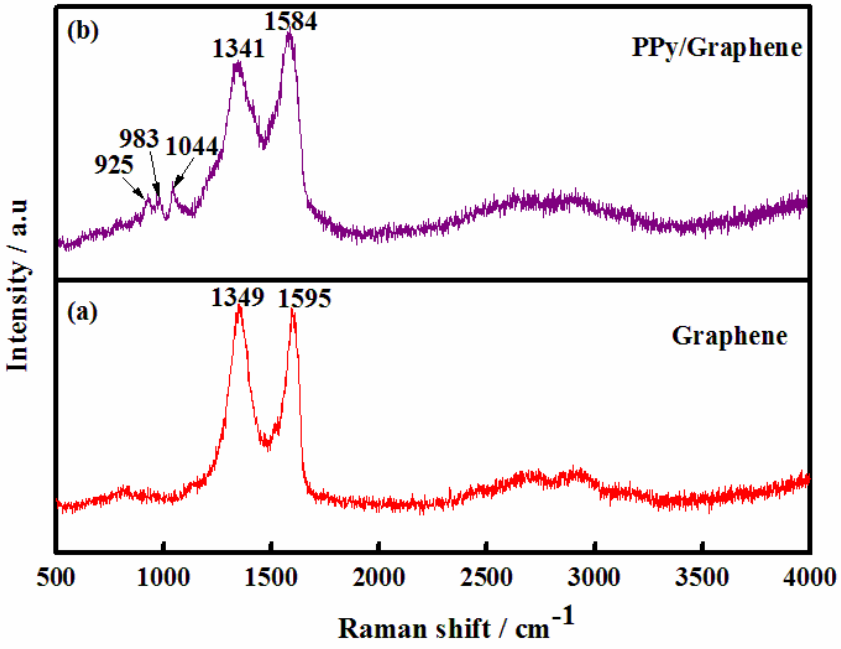

Figure 3. Raman spectra of (a) graphene layers and (b) graphene/PPy 80 wt.%.

The existence of PPy nanoparticles on the graphene layers was further investigated via Raman spectroscopy, as portrayed in Fig. 3. For this purpose, sample with the highest amount of PPy was used, which is graphene/PPy 80 wt.%. For graphene, the peaks located at 1349 and 1595 cm^{-1}, correspond to the D and G bands, respectively. The D band corresponds to the first-order Raman scattering of the E_{2g} vibrational mode, while the G band is related to the in-plane vibration of sp^2-hybridised carbon [34]. For graphene/PPy 80 wt.%, the band at 1044 cm^{-1} is attributed to the C-H in plane deformation, whereas two small peaks located at 925 cm^{-1} and 983 cm^{-1} can be assigned to the ring deformation of the quinoid polaronic and bipolaronic structure, respectively [35, 36]. The G and D bands of graphene shifted to lower wavelength due to the interaction between PPy nanoparticles and graphene layers [37].

The surface morphology of the samples was determined using SEM, as displayed in Fig. 4. From Fig. 4(a), the PPy were composed of nanoparticles with diameter approximately 0.19 μm. Graphene layers exhibited a typical morphology; crumples and wrinkles on the smooth surface with a very thin layer, as shown in Fig. 4(b). After decorated with PPy nanoparticles (Fig. 4(c-e)), the graphene retained its layer structures.

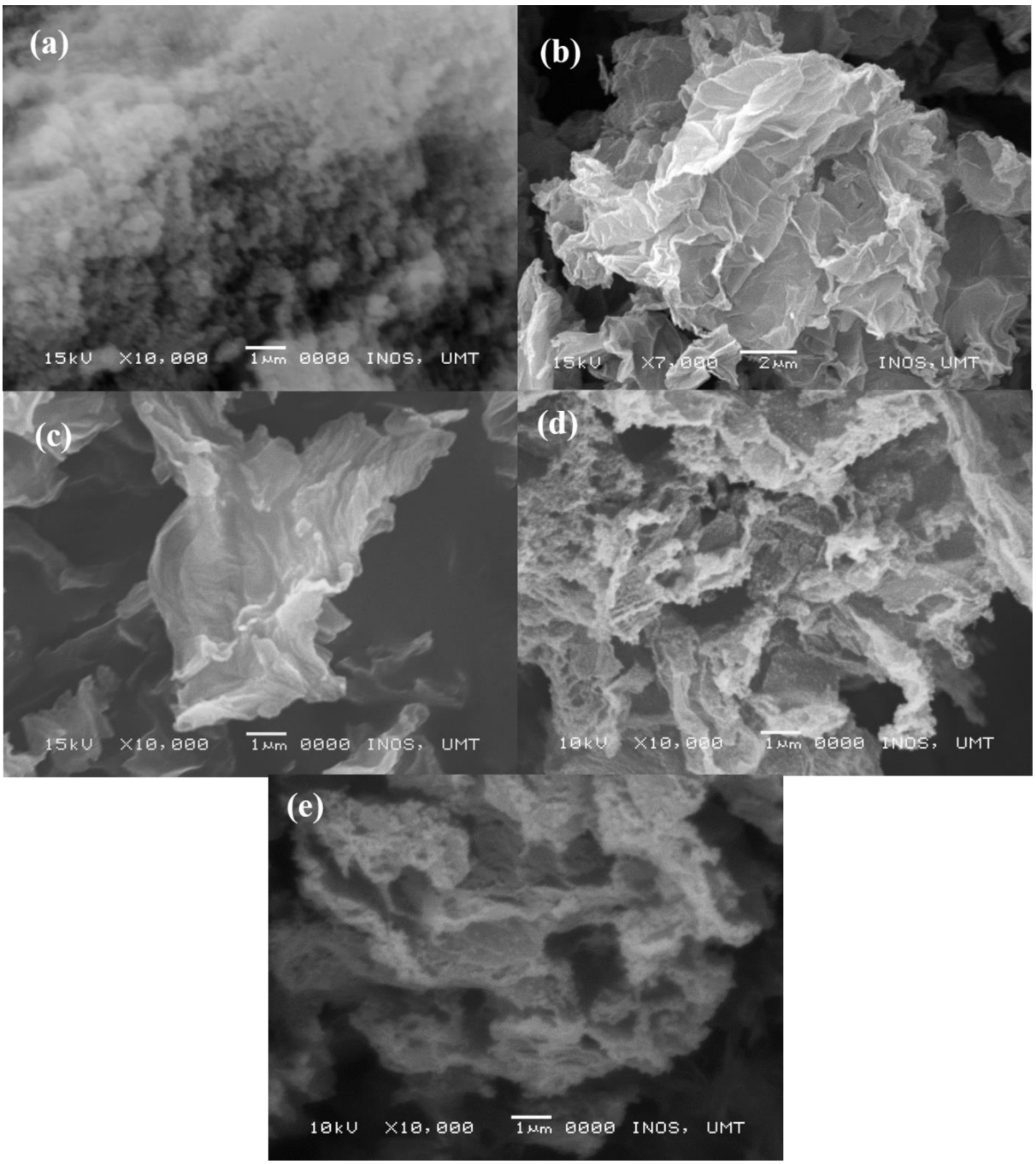

Figure 4. SEM images of (a) PPy nanoparticles (b) graphene layers, (c) graphene/PPy 20 wt.%. (d) graphene/PPy 40 wt.% and (e) graphene/PPy 80 wt.%.

The PPy nanoparticles cannot be seen clearly on the graphene layers; however, one can see that the graphene surface turned rough, when compared to the pristine graphene layers. When the amount of PPy nanoparticles were increased, the roughness of the surface of graphene layers became clearer, as shown in Fig. 4(d,e); indicating more PPy nanoparticles deposited on the surface. The deposition of PPy nanoparticles on the graphene layers can be explained through this mechanism; when pyrrole is added to a graphene suspension, weak charge-transfer complex could be formed because graphene layers are an electron acceptor, while polymer monomer (pyrrole) is an electron donor. Therefore, the monomer

could immediately get absorbed onto the surface of graphene layers due to the electrostatic interactions and the strong π-π interaction between PPy nanoparticles and graphene layers [25]. The morphology of the graphene/PPy composites was further investigated via TEM, as displayed in Fig. 5. From Fig. 5(a), wrinkles and crumpled layers were observed on the smooth surface of graphene. The surface of graphene layers were covered with protuberances (Fig. 5(b)), attributed to the formation of PPy nanoparticles on the surface, due to the strong π-π interaction between PPy nanoparticles and graphene layers [25, 38].

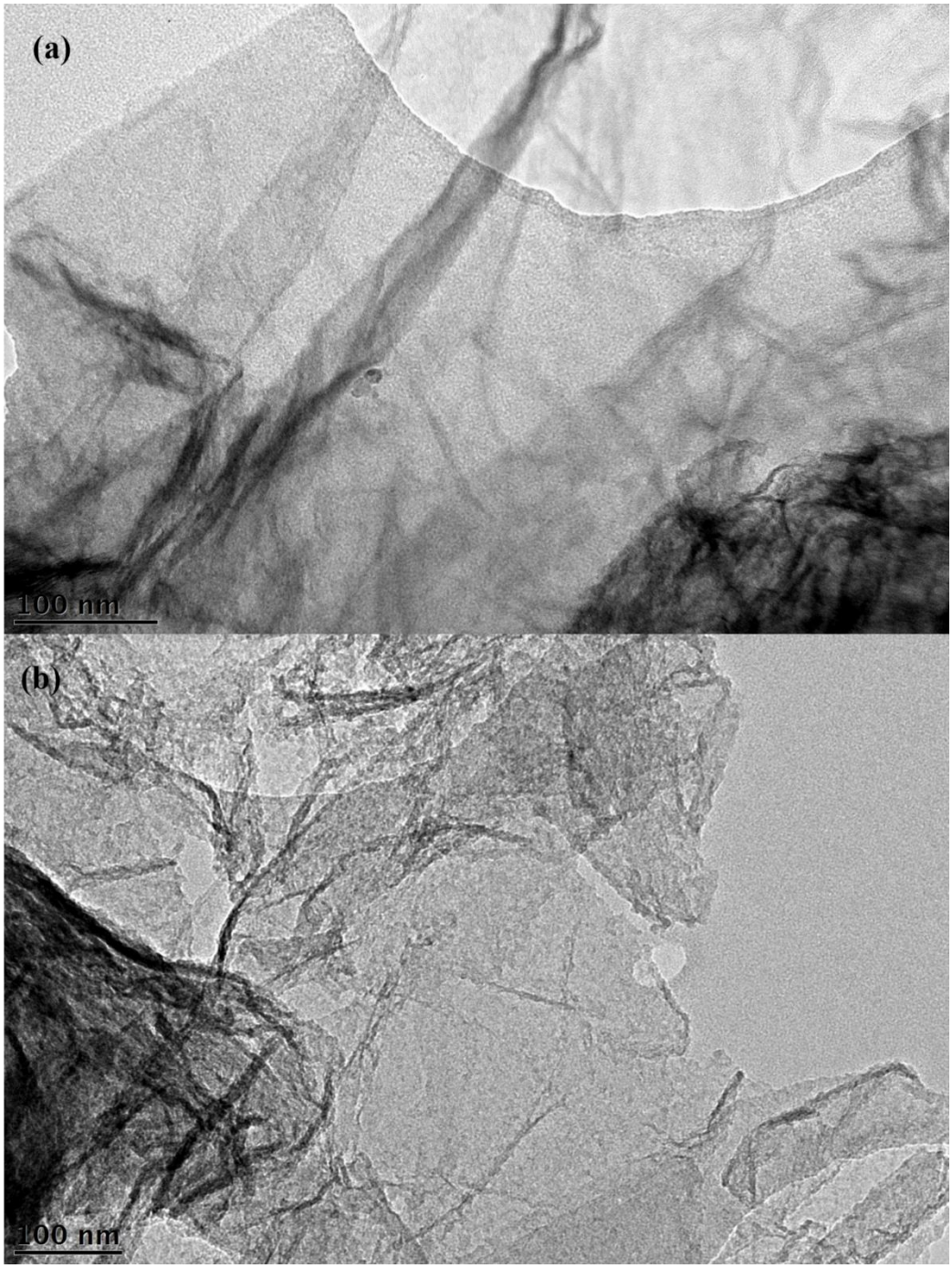

Figure 5. TEM images of (a) graphene layers and (b) graphene/PPy 80 wt.%.

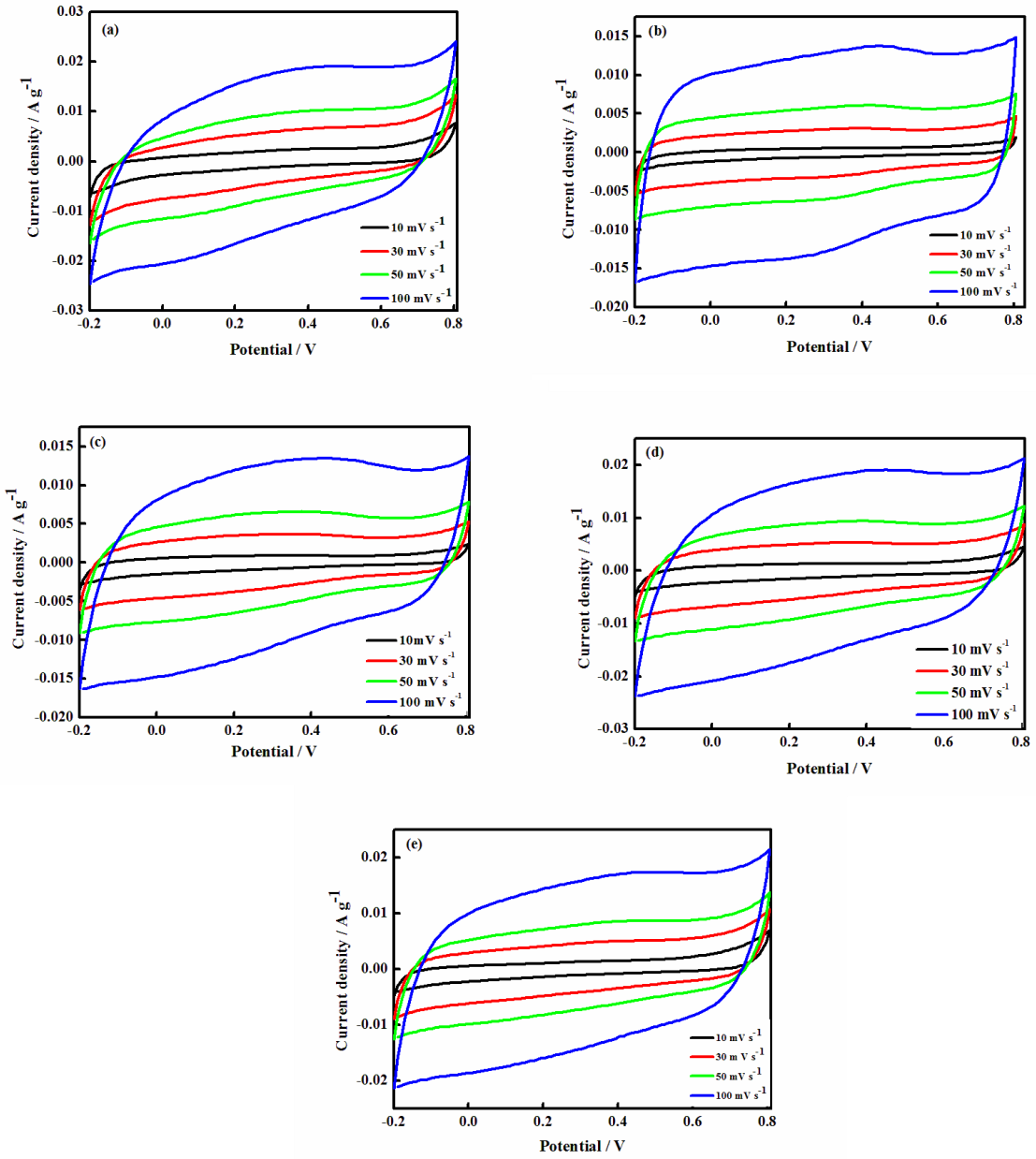

Figure 6. CV curves of (a) PPy nanoparticles, (b) graphene layers, (c) graphene/PPy 20 wt.%, (d) graphene/PPy 40 wt.% and (e) graphene/PPy 80 wt.% at different scan rates.

The cyclic voltammetry (CV) was conducted in a three-electrode system to investigate the electrochemical performances of the samples of the electrode materials, as shown in Fig. 6. Different scan rates were used i.e., 10, 30, 50, and 100 mV s^{-1} in a potential range of -0.2 until 0.8 V. From Fig. 6(a), the CV curves of PPy nanoparticles displayed a near rectangular shape and no redox peak was detected, similar to the results reported by Liu et al. [32], Fu et al. [39], and Biswas and Drzal [19]. The CV curves of graphene layers (Fig. 6(b)) exhibited nearly rectangular shape, which is the response of an ideal capacitor [40]; indicating a double-layer capacitive behaviour [41]. From Fig. 6(c-e), the CV curves were observed for the graphene/PPy composites practically rectangular shape. In addition, no clear redox peak was noted within the potential range. These composites also revealed a near rectangular shape at

high scan rate; suggesting good capacitive properties [42]. Meanwhile, Fig. 7 illustrates the CV curves of the samples at a selected number of cycles at a scan rate of 100 mV s^{-1}. Obviously, these electrodes preserved almost rectangular shape even they were cycled up to 50 cycles. Their good electrochemical activity reflects the improvement in mechanical strength and electrical conductivity of the electrodes.

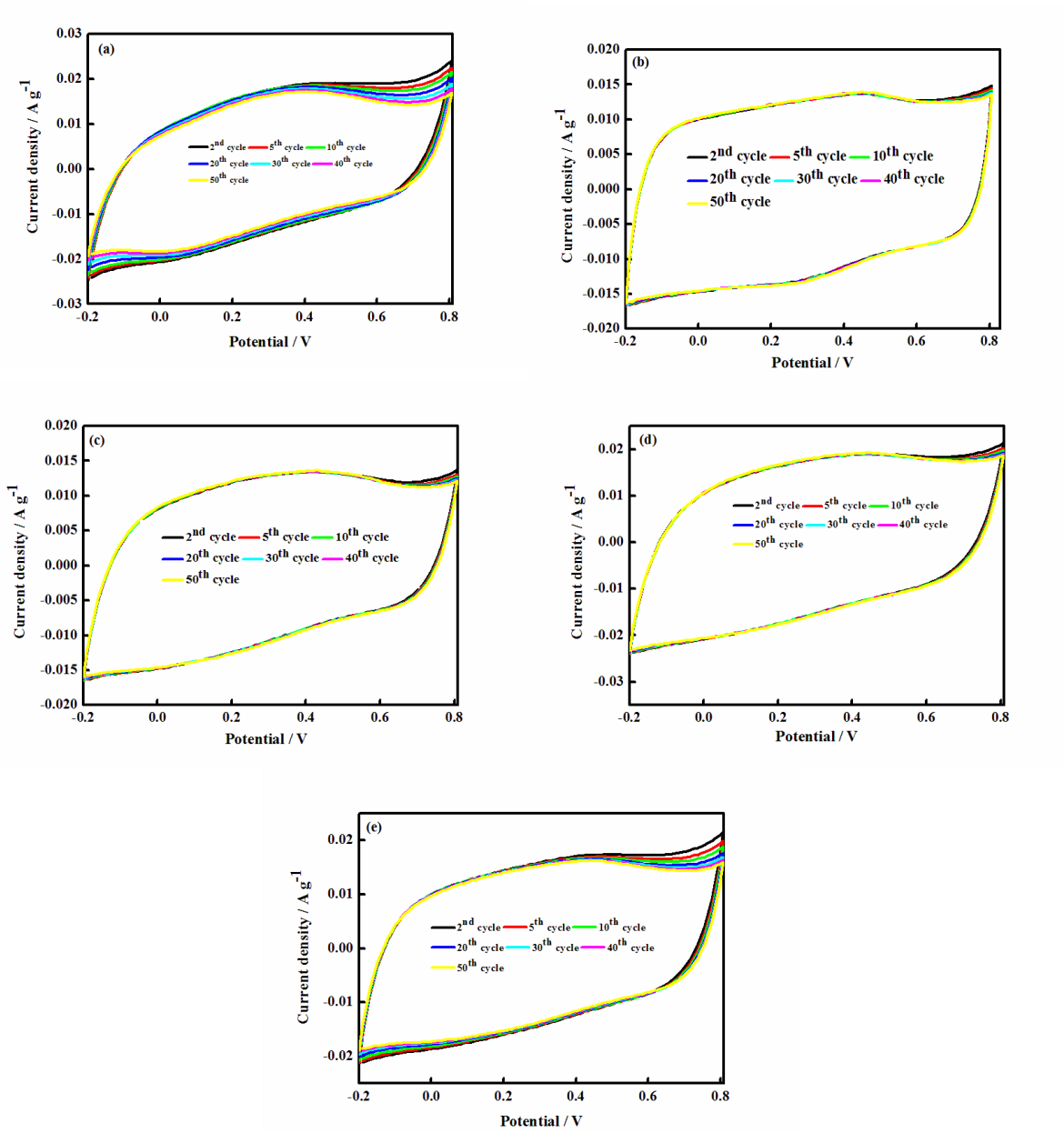

Figure 7. CV curves of (a) PPy nanoparticles, (b) graphene layers, (c) graphene/PPy 20 wt.%, (d) graphene/PPy 40 wt.% and (e) graphene/PPy 80 wt.% at selected cycles.

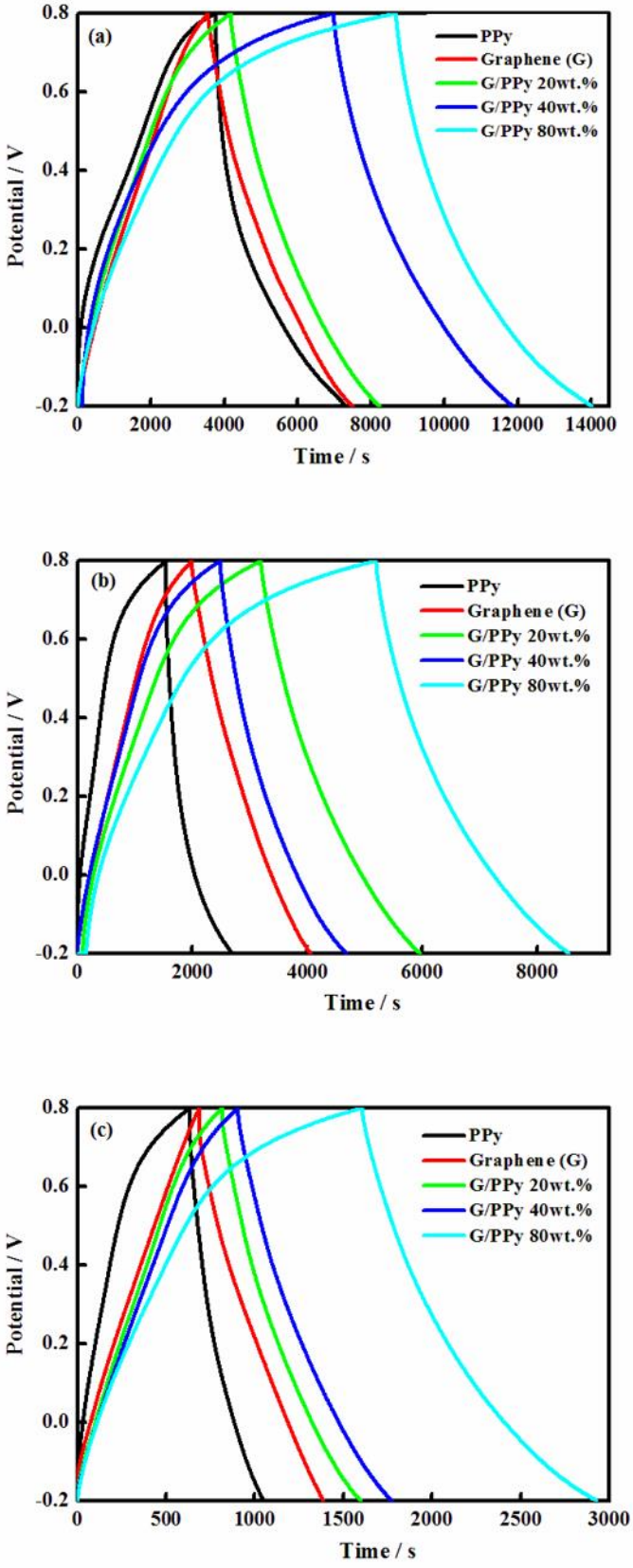

Figure 8. Galvanostatic charge/discharge curves for all electrodes at a current density of (a) 500 mA g^{-1}, (b) 1000 mA g^{-1} and 2000 mA g^{-1}.

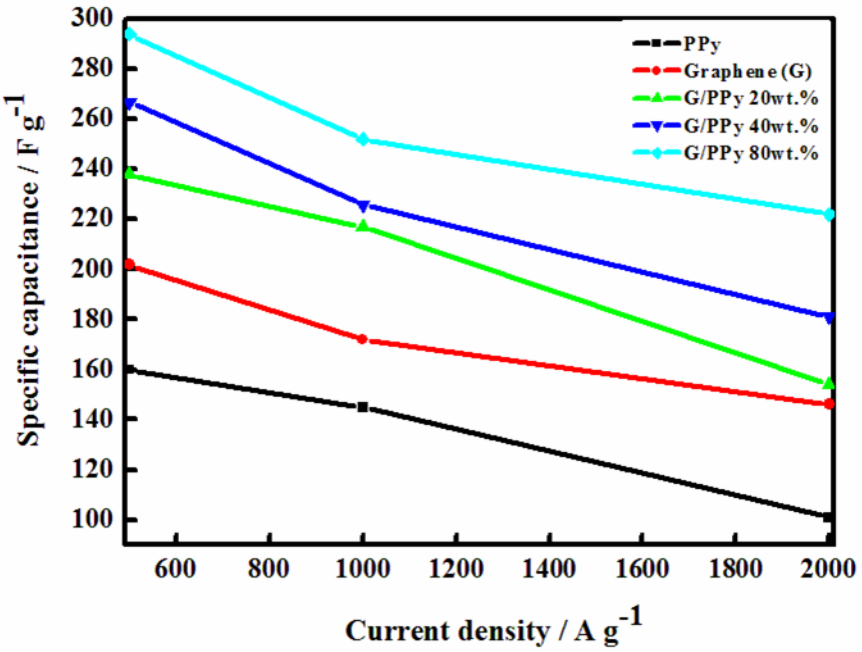

Figure 9. The plots of specific capacitance vs. current density for PPy nanoparticles, graphene layers, graphene/PPy 20 wt.%, graphene/PPy 40 wt.% and graphene/PPy 80 wt.%.

The galvanostatic charge/discharge test was conducted to calculate the specific capacitance of the samples at various current densities. All electrodes exhibited asymmetrical triangular curves (Fig. 8), which indicated good capacitive behaviour due to the presence of pseudocapacitive PPy [43]. Not only that, the discharge time of graphene/PPy 80 wt.% was longer than that of the other samples; indicating high energy stored in the electrode. The specific capacitances of all electrodes were calculated using the following equation (1):

$$C_{sp} = \frac{I\Delta t}{m\Delta V} \quad (1)$$

where, I is the discharge current (A), Δt is the discharge time (s), m is the weight of the active material (g), and ΔV is the potential range (V). Graphene/PPy 80 wt.% exhibited the highest specific capacitance compared to the other electrodes, as shown in Fig. 9; indicating that 80 wt.% PPy is the optimum weight for the graphene/PPy composites. This composite also could achieve high specific capacitance even at high current density.

Table 2. The specific capacitance of all electrodes at different current densities.

Current density / mA g^{-1}	Specific capacitance / F g^{-1}				
	PPy	Graphene	Graphene/PPy 20wt.%	Graphene/PPy 40wt.%	Graphene/PPy 80wt.%
500	160	203	213	251	270
1000	145	172	191	207	230
2000	101	144	155	181	222

Table 2 lists the specific capacitances for all electrodes at several current densities. Typically, the specific capacitance decreases as current density increases due to low current density, wherein ions are completely diffused into the inner active sites in the materials to undergo complete redox transitions. However, at high current density, ions are difficult to diffuse completely into the inner active sites in the materials, and therefore, cannot make full use of inner surface area [43].

The cyclability of the samples was studied for 1000 cycles at a current density of 5000 mA g^{-1}. As shown in Fig. 10, the capacitive retention for PPy nanoparticles was gradually decreased from 100% to 29% after 1000 cycles, while the capacitive retention for graphene layers decreased to 44%. Obviously, graphene/PPy 80 wt.% improved its cyclability with a capacitive retention of ~77% after 1000 cycles, due to the robust support of the graphene layers, where the embedded effect enhanced the mechanical strength of the composites and prevented a structural collapse that could be caused by the volumetric interchange of PPy nanoparticles [44, 45]. The capacitive retention of graphene/PPy 20 wt.% was ~50 % and ~66 % for graphene/PPy 40 wt.%. Thus, the distribution of PPy nanoparticles on the surface of graphene layers can prevent the damage of conducting polymer backbone and effectively improve the stability.

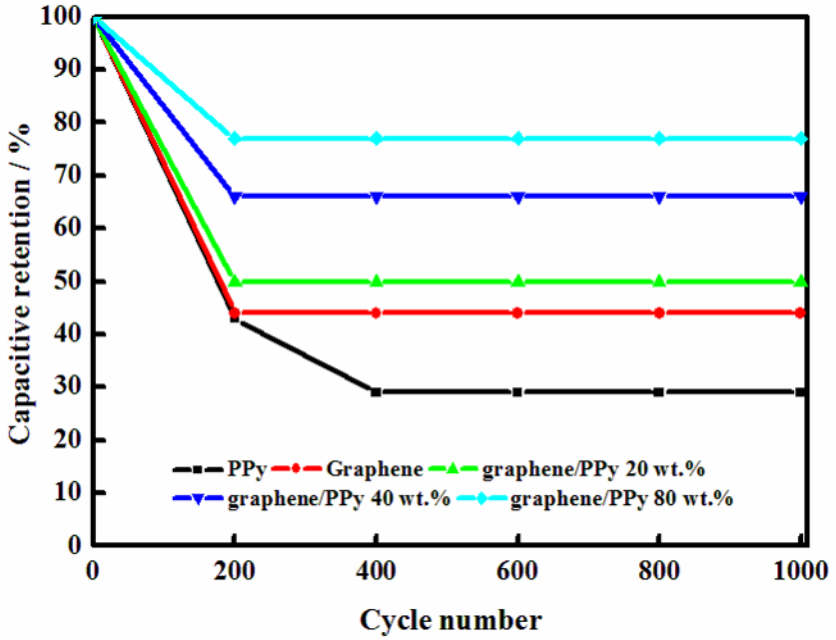

Figure 10. Cyclability of PPy nanoparticles, graphene layers and graphene/PPy composites electrodes at a current density of 5000 mA g^{-1}.

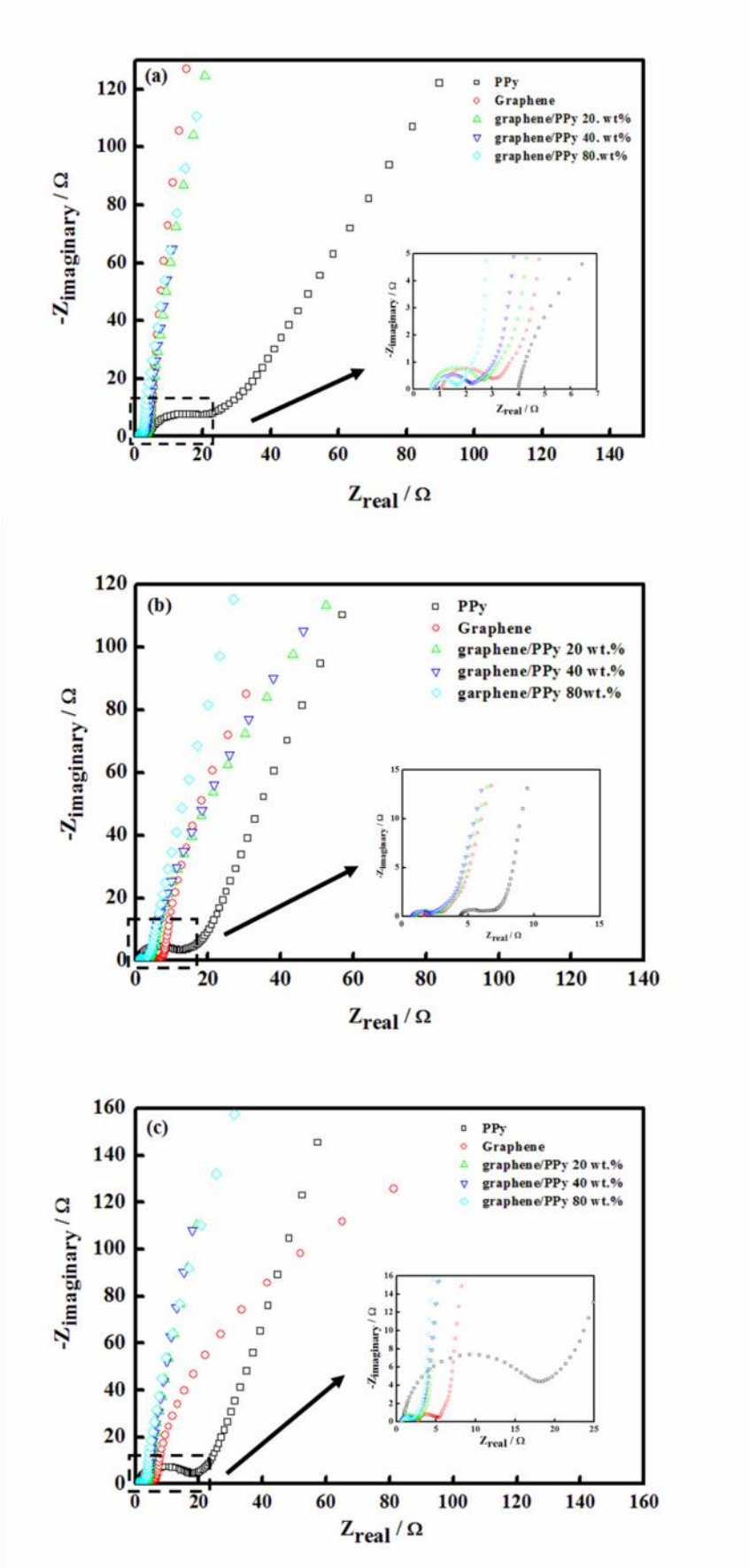

Figure 11. The Nyquist plot of all electrodes at (a) 500, (b) 1000 and (c) 2000 mA g^{-1}.

The improved electrical conductivity with the distribution of PPy nanoparticles on the graphene layers was also evidenced from impedance analysis. Nyquist plots for all electrodes are illustrated in Fig. 11 and the charge-transfer resistance (R_{ct}) values for all samples are tabulated in Table 3.

Table 3. R_{ct} values for all electrode at various current densities.

Current density/ mA g^{-1}	R_{ct} value / Ω				
	PPy	Graphene	Graphene/PPy 20wt.%	Graphene/PPy 40wt.%	Graphene/PPy 80wt.%
500	15.02	1.40	1.36	1.30	0.98
1000	11.73	1.73	1.61	1.43	1.27
2000	16.34	2.89	2.26	1.87	1.63

The graphene/PPy 80 wt.% exhibited the smallest semicircle at the middle-frequency region, which indicated the smallest R_{ct} resulting in improved rate of electrons transfer [32]. In addition, this composite shows more vertical lines for Zw in the low-frequency region at current density values of 500 mA g^{-1} (Fig. 11(a)), 1000 mA g^{-1} (Fig. 11(b)), and 2000 mA g^{-1} (Fig. 11(d)), when compared to other composites electrodes; indicating close resemblance to an ideal capacitor [32].

Overall, the addition of PPy nanoparticles into the graphene/PPy composites demonstrates an improvement in the electrochemical performances. A facile method was used to synthesise PPy/graphene composites using $FeCl_3$ as an oxidant agent and deionised water as the medium. During the polymerisation process, pyrrole monomers were attracted to the graphene layers surfaces owing to the strong π-π stacking interaction, hydrogen bonds, and Van der Walls forces between one-atom-thick planar sheets of sp^2-bonded carbon atoms (graphitic structure) of graphene layers, as displayed in Fig. 12 [46].

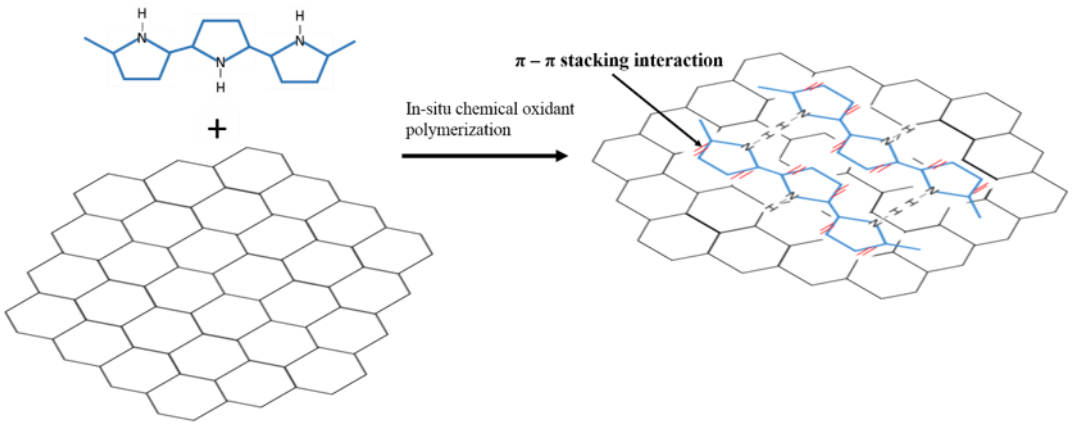

Figure 12. Formation process of PPy nanoparticles on the surface of graphene layers through *in-situ* polymerization process.

When $FeCl_3$ was introduced, PPy formed and were distributed on the graphene layers. The distribution of PPy at different weight ratios could lead to varied electrochemical performances, which can be understood by the synergistic effect between graphene layers and PPy nanoparticles. The pseudocapacitance that arises from PPy nanoparticles improves the charge storage in the graphene/PPy composites. In addition, the 0-D structure of PPy nanoparticles provides a relatively short diffusion path to improve the cycling stability and the capacitance of the electrodes [47]. The PPy has large volumetric swelling and shrinking during charge/discharge. This volumetric often leads to structural breakdown to result in fast capacitance decay of PPy. The strong attachment between graphene layers and PPy nanoparticles could enhance the mechanical strength of the composite materials, and thus, may increase the charge/discharge cycles. Furthermore, PPy nanoparticles act as a spacer that keeps the bundle of graphene layers from restacking. Graphene tends to form agglomerates and restack in multi-layer via Van der Waals interaction [48] and this problem could be prevented by introducing a spacer in the graphene interlayers [49]. In conclusion, such nanostructured composites possesses unique properties, such as large accessible area and shorter diffusion pathway for ions and electrons transportation, buffered mechanical stress during cycling, reduction in R_{ct} of electrolyte ions, and increase in electrical conductivity [50]. The concept introduced in this research work is valuable to the realisation of high performance electrode materials for supercapacitors.

4. CONCLUSION

Graphene layers and PPy nanoparticles were prepared using *in-situ* polymerization method. By tuning the weight ratios of the PPy nanoparticles and the graphene layers, graphene/PPy composites with different compositions were prepared, where graphene/PPy 80 wt.% exhibited the highest electrochemical properties. The morphology and the structure of these composites, together with PPy nanoparticles and graphene layers, were characterised with varied techniques, including XRD, FTIR, Raman spectroscopy, SEM, and TEM. It is evident that the distribution of PPy nanoparticles on the graphene layers does not only increase the surface area of the hybrid materials, but also facilitates fast charge-transfer, resulting in enhanced rate capability. The highest specific capacitance and good cycling stability were achieved for graphene/PPy 80wt.% with specific capacitance of 270 F g^{-1} at a current density of 500 mA g^{-1}. These results revealed that the synergetic effect contributed from graphene layers and PPy nanoparticles can significantly improve the electrochemical properties of the composites.

ACKNOWLEDGEMENT
Financial support was provided by the Universiti Malaysia Terengganu through a Talent and Publication Enhancement-Research Grant (TAPE-RG) (Vote no. 55158) and MyBrain15 scholarship sponsored to the student is gratefully acknowledged.

References

1. L.L. Zhang, X.S. Zhao, *Chem. Soc. Rev.*, 38 (2009) 2520-2531.

2. E. Frackowiak, *Phys. Chem. Chem. Phys.*, 9 (2007) 1774-1785.
3. P. Simon, Y. Gogotsi, *Nat. Mater.*, 7 (2008) 845-854.
4. Z. Niu, W. Zhou, J. Chen, G. Feng, H. Li, W. Ma, J. Li, H. Dong, Y. Ren, D. Zhao, S. Xie, *Energy Environ. Sci.*, 4 (2011) 1440-1446.
5. J.-L. Shi, W.-C. Du, Y.-X. Yin, Y.-G. Guo, L.-J. Wan, *J. Mater. Chem. A*, 2 (2014) 10830-10834.
6. H. Jiang, P.S. Lee, C. Li, *Energy Environ. Sci.*, 6 (2013) 41-53.
7. D.-W. Wang, F. Li, M. Liu, G.Q. Lu, H.-M. Cheng, *Angew. Chem.*, 120 (2008) 379-382.
8. C. Ji, S. Kaixuan, L. Peihui, L. Chun, S. Gaoquan, *Adv. Mater.*, 24 (2012) 4569-4573.
9. S.H. Aboutalebi, R. Jalili, D. Esrafilzadeh, M. Salari, Z. Gholamvand, S. Aminorroaya Yamini, K. Konstantinov, R.L. Shepherd, J. Chen, S.E. Moulton, P.C. Innis, A.I. Minett, J.M. Razal, G.G. Wallace, *ACS Nano*, 8 (2014) 2456-2466.
10. P. Hao, Z. Zhao, J. Tian, H. Li, Y. Sang, G. Yu, H. Cai, H. Liu, C.P. Wong, A. Umar, *Nanoscale*, 6 (2014) 12120-12129.
11. A. Halama, B. Szubzda, G. Pasciak, *Electrochim. Acta*, 55 (2010) 7501-7505.
12. R. Saliger, U. Fischer, C. Herta, J. Fricke, *J. Non-Cryst. Solids*, 225 (1998) 81-85.
13. C. Liu, Z. Yu, D. Neff, A. Zhamu, B.Z. Jang, *Nano Lett.*, 10 (2010) 4863-4868.
14. Y.B. Tan, J.-M. Lee, *J. Mater. Chem. A*, 1 (2013) 14814-14843.
15. Y. Wang, Z. Shi, Y. Huang, Y. Ma, C. Wang, M. Chen, Y. Chen, *J. Physc. Chem. C*, 113 (2009) 13103-13107.
16. R.-R. Bi, X.-L. Wu, F.-F. Cao, L.-Y. Jiang, Y.-G. Guo, L.-J. Wan, *J. Physc. Chem. C*, 114 (2010) 2448-2451.
17. M.-S. Wu, Y.-R. Zheng, G.-W. Lin, *Chem. Commun.*, 50 (2014) 8246-8248.
18. R.B. Rakhi, W. Chen, M.N. Hedhili, D. Cha, H.N. Alshareef, *ACS Appl. Mater. Interfaces*, 6 (2014) 4196-4206.
19. S. Biswas, L.T. Drzal, *Chem. Mater.*, 22 (2010) 5667-5671.
20. F. L.-Z., H. Y.-S., M. J., A. P., S. B., A. M., *Adv. Funct. Mater.*, 17 (2007) 3083-3087.
21. M.H. Chakrabarti, C.T.J. Low, N.P. Brandon, V. Yufit, M.A. Hashim, M.F. Irfan, J. Akhtar, E. Ruiz-Trejo, M.A. Hussain, *Electrochim. Acta*, 107 (2013) 425-440.
22. W. Y.-G., L. H.-Q., X. Y.-Y., *Adv. Mater.*, 18 (2006) 2619-2623.
23. K. Igor, B.D. G., Y. Gleb, *Adv. Funct. Mater.*, 20 (2010) 3979-3986.
24. G.A. Snook, P. Kao, A.S. Best, *J. Power Sources*, 196 (2011)
25. J. Zhang, X.S. Zhao, *J. Physc. Chem. C*, 116 (2012) 5420-5426.
26. Y. Zhang, Y.-W. Tan, H.L. Stormer, P. Kim, *Nature*, 438 (2005) 201.
27. A.A. Balandin, S. Ghosh, W. Bao, I. Calizo, D. Teweldebrhan, F. Miao, C.N. Lau, *Nano Lett.*, 8 (2008) 902-907.
28. C. Lee, X. Wei, J.W. Kysar, J. Hone, *Science*, 321 (2008) 385.
29. W.S. Hummers, R.E. Offeman, *J. Am. Chem. Soc.*, 80 (1958) 1339-1339.
30. T.K. Vishnuvardhan, V.R. Kulkarni, C. Basavaraja, S.C. Raghavendra, *Bull. Mater. Sci.*, 29 (2006) 77-83.
31. S. Zhou, H. Zhang, Q. Zhao, X. Wang, J. Li, F. Wang, *Carbon*, 52 (2013) 440-450.
32. Y. Liu, H. Wang, J. Zhou, L. Bian, E. Zhu, J. Hai, J. Tang, W. Tang, *Electrochim. Acta*, 112 (2013) 44-52.
33. X. Zhang, J. Zhang, W. Song, Z. Liu, *J. Phys. Chem. B*, 110 (2006) 1158-1165.
34. A.C. Ferrari, J.C. Meyer, V. Scardaci, C. Casiraghi, M. Lazzeri, F. Mauri, S. Piscanec, D. Jiang, K.S. Novoselov, S. Roth, A.K. Geim, *Phys. Rev. Lett.*, 97 (2006) 187401.
35. X. Fan, Z. Yang, N. He, *RSC Adv.*, 5 (2015) 15096-15102.
36. G. Han, J. Yuan, G. Shi, F. Wei, *Thin Solid Films*, 474 (2005) 64-69.
37. V. Chandra, K.S. Kim, *Chem. Commun.*, 47 (2011) 3942-3944.
38. Q. Yao, L. Chen, W. Zhang, S. Liufu, X. Chen, *ACS Nano*, 4 (2010) 2445-2451.
39. H. Fu, Z.-j. Du, W. Zou, H.-q. Li, C. Zhang, *J. Mater. Chem. A*, 1 (2013) 14943-14950.

40. C. Xu, J. Sun, L. Gao, *J. Mater. Chem.*, 21 (2011) 11253-11258.
41. K. Zhang, L.L. Zhang, X. Zhao, J. Wu, *Chem. Mater.*, 22 (2010) 1392-1401.
42. D. Zhang, X. Zhang, Y. Chen, P. Yu, C. Wang, Y. Ma, *J. Power Sources*, 196 (2011) 5990-5996.
43. P.K. Kalambate, R.A. Dar, S.P. Karna, A.K. Srivastava, *J. Power Sources*, 276 (2015) 262-270.
44. G. Wang, L. Zhang, J. Zhang, *Chem. Soc. Rev.*, 41 (2012) 797-828.
45. H.-P. Cong, X.-C. Ren, P. Wang, S.-H. Yu, *Energy Environ. Sci.*, 6 (2013) 1185-1191.
46. Y.-m. Cai, Z.-y. Qin, L. Chen, *Prog. Nat. Sci. Mater. Int.*, 21 (2011) 460-466.
47. S. Chen, H. Liu, Y. Wang, S. Xu, W. Liu, D. He, X. Liu, J. Liu, C. Hu, *Electrochim. Acta*, 232 (2017) 72-79.
48. D. Li, M.B. Müller, S. Gilje, R.B. Kaner, G.G. Wallace, *Nat. Nanotechnol.*, 3 (2008) 101.
49. R.B. Rakhi, H.N. Alshareef, *J. Power Sources*, 196 (2011) 8858-8865.
50. L.-L. Zhang, H.-H. Li, C.-Y. Fan, K. Wang, X.-L. Wu, H.-Z. Sun, H.-M. Xie, J.-P. Zhang, *Electrochim. Acta*, 184 (2015) 179-185.
51. H.-H. Chang, C.-K. Chang, Y.-C. Tsai, C.-S. Liao, *Carbon*, 50 (2012) 2331-2336.
52. J. Liu, J. An, Y. Ma, M. Li, R. Ma, *J. Electrochem. Soc.*, 159 (2012) A828-A833.
53. Y. Liu, Y. Zhang, G. Ma, Z. Wang, K. Liu, H. Liu, *Electrochim. Acta*, 88 (2013) 519-525.
54. Y. Song, J.-L. Xu, X.-X. Liu, *J. Power Sources*, 249 (2014) 48-58.